Diffusion Monte Carlo Approaches to the Study of the Rotationally Excited States of H_3^+ and H_2D^+

Honors Research Thesis

Presented in Partial Fulfillment of the Requirements for Graduation
"with Honors Research Distinction in Chemistry" in the Undergraduate
Colleges of The Ohio State University

by
Bethany Wellen

The Ohio State University
May 2013

Project Advisor: Professor Anne B. McCoy, Department of Chemistry and Biochemistry

ABSTRACT

Diffusion Monte Carlo (DMC) has been shown to be a successful technique for treating the quantum zero-point effects of floppy molecules and clusters. Here, we report the results of our fixed-node DMC methodology when applied to the model systems H_3^+ and H_2D^+. The fixed-node approach has been developed to account for the nodes in the wave functions of rotationally excited states. The accuracy of our fixed-node DMC studies will be examined and compared with other methods. In particular, a comparison with converged variational calculations provides the most thorough test of the effectiveness of our methodology over a large range of quantum states. The fixed-node DMC methodology produces more accurate energetic calculations than evaluations using a rigid rotor model of the excited states of fluxional molecules.

INTRODUCTION

High resolution, rotationally resolved spectroscopy is used to identify and study the molecular species that exist in diffuse interstellar clouds.[1] The rovibrational spectrum of many molecules, including H_3^+ and H_2D^+, is not as easily defined using the theory taught in introductory physical chemistry courses as that of a simple molecule, say HCl.[2] Figure 1 is the rotational spectrum of HCl taken in the Physical Chemistry Lab course at Ohio State. The P and R branches can easily distinguish the spectrum.

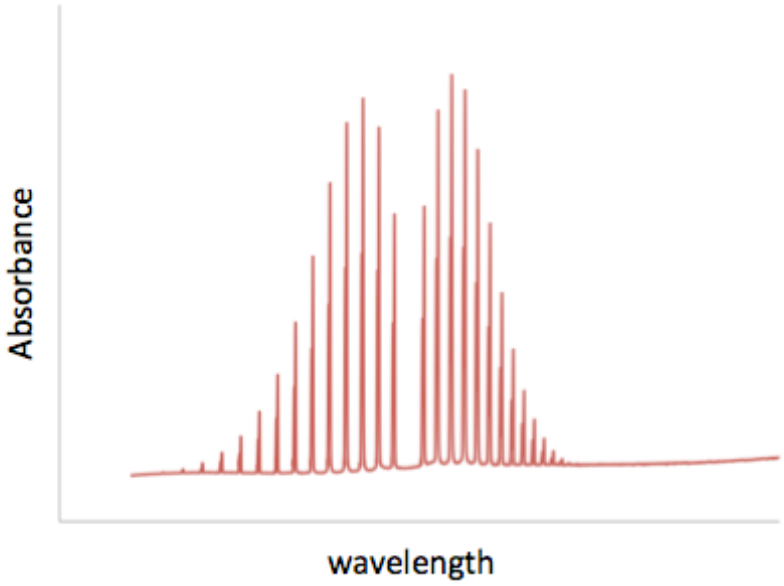

Figure 1: The rotational spectrum of HCl is easily defined.

Theoretical studies help spectroscopists identify relevant spectral ranges, in terms of energy, in which to look for the molecules of interest by calculating the energies of the system in the ground as well as in excited states. This helps the experimentalist to assign and interpret spectra.

Spectroscopic studies have shown that the rotationally excited states of molecular species can often be well described by Hamiltonians of the form

(1) $$\hat{H}_{rot} = A_v \hat{J}_A^2 + B_v \hat{J}_B^2 + C_v \hat{J}_C^2.$$

One of the underlying assumptions in using this Hamiltonian is that the system can be treated as a simple rigid rotor. However, large amplitude vibrational motion causes this assumption to break down due to the coordinate dependence of the rotational constants, thus preventing the perturbative expansion of the Hamiltonian from converging onto an accurate solution.[3]

The limitations of perturbation theory are circumvented by the use of variational calculations. While converged variational calculations of spectroscopic accuracy for molecules of 3 or 4 atoms have been reported, the computational cost of such calculations is great compared to the relatively small size of the system. When the system exhibits large amplitude vibrational motion, this problem becomes much worse in terms of calculation time and the increased number of variables that need to be considered. Therefore, converged variational calculations of fluxional molecules and clusters are quite challenging.[3]

Diffusion Monte Carlo (DMC) provides a useful alternative to the variational approach when studying the nature of rotation-vibration coupling in the rotationally excited states of floppy molecules and clusters.[4,5] Originally developed as a method for the study of ground state systems, the fixed-node approximation has allowed DMC to be extended so that excited states can also be studied. In the fixed-node approximation, originally introduced by Anderson, a DMC calculation is used to evaluate the lowest energy state consistent with a set of nodal surfaces obtained from either symmetry considerations or model calculations (i.e. the rigid rotor model).[3-5] Fixed-node DMC allows for the direct calculation of the excited state wave function, which can be analyzed to provide insights into the effect of rotational excitation on the molecule's structure and reaction dynamics.

In this work, we develop a fixed-node DMC approach to the study of the rotationally excited states of highly fluxional symmetric and asymmetric top molecules and clusters. H_3^+ and

H_2D^+ exhibit large amplitude, zero-point vibrational motion. The molecules also contain unusually large rotational constants due to the absence of heavy atoms. Both of these features suggest the presence of strong rotation-vibration coupling. These molecules are good test systems for our approach because global potential energy surfaces of high accuracy have been reported in the literature.[6-8] In addition, converged variational calculations of the ro-vibrational states to spectroscopic accuracy have also been reported.[9]

The main goal of this work is to evaluate the quality of the fixed-node DMC treatment for describing rotationally excited states of H_3^+ and H_2D^+ using the nodal surfaces obtained from rigid rotor wave functions. The results of the DMC calculations also serve to provide insight into the strength and nature or rotation-vibration coupling in the rotationally excited states of these fluxional molecules.[3]

GENERAL DIFFUSION MONTE CARLO THEORY

Diffusion Monte Carlo (DMC), as first formalized by Anderson, is a statistical approach to solving the time-independent Schrodinger equation, $\hat{H}\Psi=E\Psi$.[4,5] This equation has two variables, the energy, E, and the wave function, Ψ. To get Ψ, the time-dependent Schrodinger equation is solved in imaginary time. Before discussing the details of the approach, we consider the time-dependent Schrodinger equation.

$$i\hbar\frac{d\Psi}{dt}=\hat{H}\Psi \tag{2}$$

The Hamiltonian, $\hat{H}$, is the sum of the kinetic energy operator and the potential energy operator. In 1-D, these operators are given by

$$\hat{T}=-\frac{\hbar^2}{2m}\frac{\partial^2}{\partial x^2} \tag{3}$$

$$\hat{V}=V(x). \tag{4}$$

The general solution to the time-dependent Schrödinger equation is

$$\Psi(t)=\left(\sum_{k=0}^{\infty}e^{-iE_kt/\hbar}c_k\psi_k\right)e^{iE_{ref}t/\hbar}\ , \tag{5}$$

where $\hat{H}\Psi_k=E_k\Psi_k$, and the time evolution is found in the relative phases associated with the Ψ_k. This sum can be multiplied by a phase factor, without loss of generality. In Equation (5), we define the phase factor in terms of E_{ref}, which will ultimately be equated with E_0. The oscillating behavior of the contributions of the individual Ψ_k's to $\Psi(t)$ can be converted to decaying exponentials by working in imaginary time, τ, where $\tau=it/\hbar$. Expressed in this way the wave function can be written as[4,5]

$$\Psi(\tau)=\sum_{k=0}^{\infty}e^{-(E_k-E_{ref})\tau}c_k\psi_k\ . \tag{6}$$

If E_{ref} is equal to E_0, the ground state energy, then

(7) $$\Psi(\tau) = e^{-(E_0 - E_0)\tau} c_0 \psi_0 + \sum_{k=1}^{\infty} e^{-(E_k - E_0)\tau} c_k \psi_k .$$

Because E_k will always be greater than E_0, in the limit that τ approaches infinity, $\Psi(\tau)$ will collapse onto the ground state wave function.[10-12]

This then begs the question of how the simulation evolves over time in order to reach this limit. Recall from Equation (2) that the time dependent Schrodinger equation can be arranged as

(8) $$\frac{d\Psi}{\Psi} = -\frac{i}{\hbar}\hat{H}dt ,$$

which when integrated yields

(9) $$\Psi(t + \delta t) = e^{-i\hat{H}\delta t/\hbar}\Psi(t).$$

This form of the wave function can be rewritten via the split operator approximation as

(10) $$\Psi(t + \delta t) \approx e^{-\frac{i}{\hbar}\delta t\hat{V}} e^{-\frac{i}{\hbar}\delta t\hat{T}}\Psi(t).$$

This is an approximation because the operators $\hat{T}$ and $\hat{V}$ do not commute.[10] In imaginary time,

(11) $$\Psi(\tau + \delta\tau) \approx e^{-(\hat{V} - E_{ref})\delta\tau} e^{-\hat{T}\delta\tau}\Psi(\tau).$$

Based on this, the wave function is propagated through a series of small time steps. In DMC, Ψ is represented by an ensemble of walkers, which are mathematically represented by δ-functions. Using this representation of Ψ, Equation (11) can be solved by focusing on the evolution of individual walkers over time. The kinetic energy term in Equation (11) leads to the diffusion of the walkers. Specifically, each walker is randomly displaced in each of the 3N Cartesian coordinates based on a Gaussian distribution with width

(12) $$\sigma = \sqrt{\frac{\delta\tau}{m_i}} .$$

This expression is based on the evolution of an infinitely narrow Gaussian via the action of the $e^{-\hat{T}\delta\tau}$ term.[13] The potential energy contribution to Equation (11) leads to walker birth and death.

If over the time step, the walker moves to a region where the potential energy is larger than E_{ref}, then it has a probability of dying, and consequently being removed from the simulation. If the walker moves to a region of low potential energy, it produces additional walkers that are added to the ensemble.[3-5] In this case, where V(x), the value of the potential energy at the position of the walker, is less than E_{ref} at time τ, the number of offspring added to the ensemble is governed by

$$e^{-(V(x)-E_{ref}(\tau))\delta\tau} \equiv P > 1 \tag{13}$$

where the integer part of P determines the number of walkers added to the ensemble and the fractional part of P determines whether the original walker remains in the ensemble.[14] As the simulation proceeds, the reference energy is updated via

$$E_{ref}(\tau) = \overline{V}(\tau) - \alpha \frac{N_{walk}(\tau) - N_{walk}(0)}{N_{walk}(0)} \tag{14}$$

where $\overline{V}(\tau)$ is the ensemble average of the potential energy, $N_{walk}(\tau)$ is the number of walkers at some instant in time, τ, and α is a simulation parameter.[4]

The distribution of the walkers along the surface at the end of the simulation provides a Monte Carlo sampling of the ground state wave function. In order to calculate expectation values and probability distributions, a second copy of the wave function is required. This copy is obtained via descendent weighting.[14] As the DMC simulation proceeds, a snapshot of the wave function is taken at a series of defined times, Ψ_{DMC}. Each walker in the simulation is followed for a specified number of time steps, and the number of descendents of each walker is counted, along with the original walker from which they came. This number gives the value of Ψ_{DW} at the coordinate of the walker. These distributions provide a second copy of the wave function, Ψ_{DW}. If, for example, the average value of the variable A was of interest, then by using the equation

$\left\langle \Psi_{DMC} \middle| \hat{A} \middle| \Psi_{DW} \right\rangle$, the value of A can be calculated. Operationally, this equation can be written in the form

$$\left\langle \Psi_{DMC} \middle| \hat{A} \middle| \Psi_{DW} \right\rangle = \frac{\sum_{i=1}^{N_{walk}} \Psi_{DW}(x_i) A(x_i)}{\sum_{i=1}^{N_{walk}} \Psi_{DW}(x_i)}, \tag{15}$$

where $A(x_i)$ is evaluated at the position of the walkers. This calculation is repeated for every set of wave functions collected over the experiment. The evaluations of the wave functions are spaced out by a specified propagation time of τ. These values are then averaged together to obtain the overall average.[14]

FIXED-NODE DIFFUSION MONTE CARLO THEORY

As indicated by Equation (7), Diffusion Monte Carlo is a method for determining ground state energies and wave functions. The original DMC method requires some modifications in order for it to be used in studies of excited states. In order to account for the nodes in the excited state wave function, a fixed-node approximation is applied. The Hamiltonian is modified by placing an infinite potential barrier at the location of the node in the wave function.[10]

$$\hat{H}_{\text{mod}} = \hat{H}_0 + \begin{cases} 0, r > r_{node} \\ \infty, r \le r_{node} \end{cases} \tag{16}$$

In the fixed-node DMC simulation, the wave function goes to zero with a finite slope at the node. This way, the behavior in the vicinity of a node is similar to that of a particle in a box.

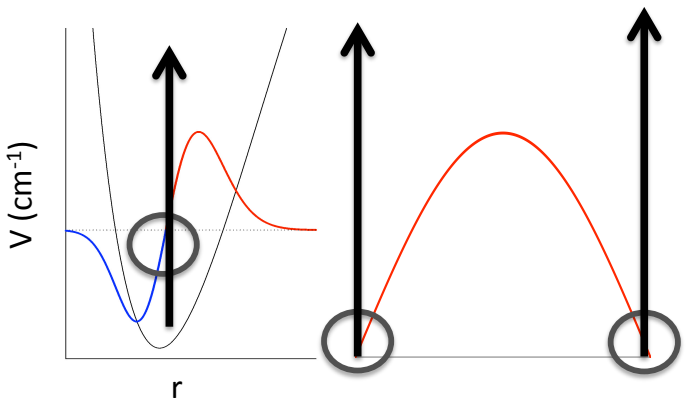

Figure 2: The behavior of a particle in a box.

The nodal surfaces that define an excited state wave function divide configuration space into a series of nodal regions. A DMC simulation is run in each nodal region. The reference energy, E_{ref}, will fluctuate around the energy of the excited state when it reaches equilibrium. The distribution of the walkers provides a Monte Carlo sampling of a portion of the excited state wave function inside of that nodal region. If the nodes are properly placed, then the average energies calculated in the different nodal regions of a particular excited state will be equal because $\hat{H}\Psi=E\Psi$ must be satisfied everywhere in configuration space.[10]

Before the DMC simulation can be performed within a nodal region, the boundaries of that region must be defined. A rigid rotor approximation is used to provide the nodal surface for rotationally excited states. First, the vibrationally averaged rotational constants need to be calculated. The inverse moment of inertia matrix, I^{-1}, is calculated at the geometry of each walker. The diagonal elements of this 3x3 matrix are the rotational constants A, B, and C. These constants are then averaged over the ground state probability amplitude to determine the vibrationally averaged rotational constants for the system,[10]

$$\langle A \rangle_0 = \frac{\langle I_{AA}^{-1} \rangle_0}{2}, \tag{17}$$

where

$$I_{AA} = \sum_{i=1}^{N_{atom}} m_i (x_{B_i}^2 + x_{C_i}^2). \quad (18)$$

In Equation (18), $(x_B + x_C)^2$ is the distance of the atom from the A-axis. The three rotational constants are then substituted into the rigid rotor Hamiltonian.[15]

$$\hat{H}_{RR} = \langle A \rangle_0 \hat{J}_A^2 + \langle B \rangle_0 \hat{J}_B^2 + \langle C \rangle_0 \hat{J}_C^2 \quad (19)$$

The eigenvalues and eigenvectors are then determined from the Hamiltonian and the eigenfunctions provide a picture of the rotational wave function of the states of interest. The nodal region is then mapped out and these coordinates are inputted into the DMC calculation as the points containing the infinite potential energy barrier.[3,10]

It is important to note that this study is conducted in the Eckart frame. H_3^+ and H_2D^+ are floppy molecules that experience large amplitude zero-point vibrations. Eckart embedding minimizes the coupling of rotational and vibrational motions. The Hamiltonian can be expressed as the sum of individual Hamiltonians for vibrations, rotations, and rovibrational motions.

$$\hat{H} = \hat{H}_{vib} + \hat{H}_{rot} + \hat{H}_{VR} \quad (20)$$

Eckart embedding minimizes the $\hat{H}_{VR}$ term in Equation (20). The fixed-node approximation relies on the assumption that the nodal surfaces of the rotationally excited states are only dependent on rotational coordinates, and thus $\hat{H}_{rot}$ can be solved independently with the rigid rotor approximation.[10] Figure 3 is the nodal surface of one of the rotationally excited states of H_3^+. It can be seen that the coordinates for the rigid rotor wave function are the Euler angles θ and χ.

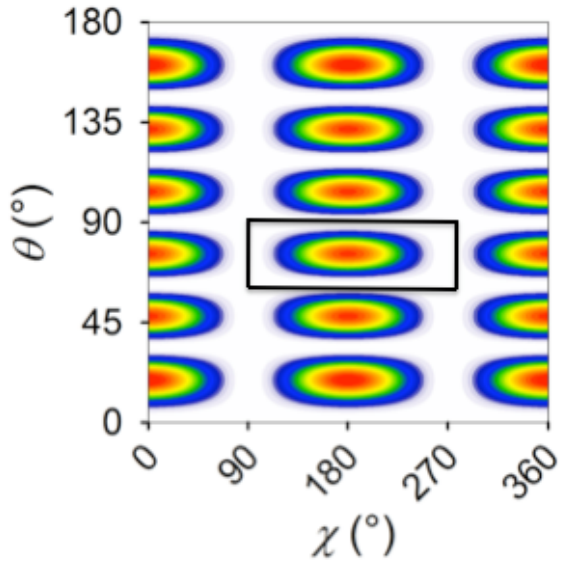

Figure 3: Contour plot of the $|6,1,0\rangle_+$ state of H_3^+. The black box represents the boundary surface containing the infinite potential barrier that was inputted into the DMC simulation.[10]

The Euler angles describe the orientation of the molecule with respect to a space-fixed axis. While the angles describe the molecular orientation in space, the quantum numbers J and K describe the total angular momentum and the projection of that angular momentum onto a body-fixed axis. These axes and angles can be seen in Figure 4. In symmetric top systems, like H_3^+, rotationally excited states are labeled in the form $|J,K,M\rangle_\pm$, where the M quantum number in our study is equal to zero because there is no external field. Asymmetric top molecules are labeled in the form J_{K_A,K_C}, where K_A is the projection of the angular momentum onto the body-fixed A-axis and K_C is the projection onto the body-fixed C-axis.

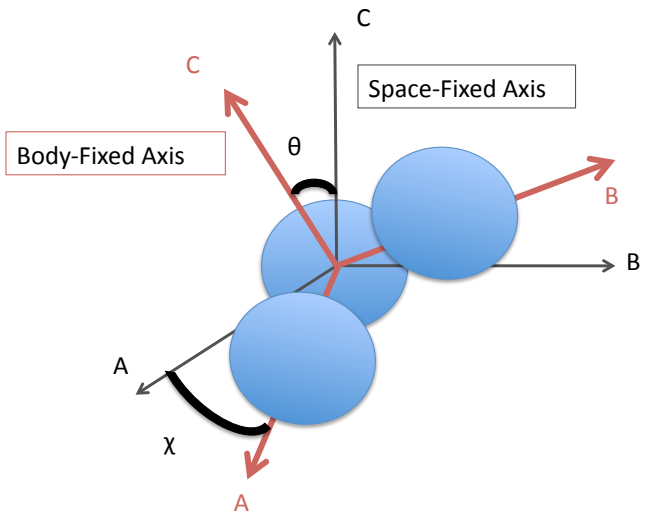

Figure 4: Rotational coordinates and axis systems

Because a finite time step is used in this study, there must exist a correction for the possibility of a walker crossing and recrossing the nodal surface, where the potential energy is infinite, within that time step, as illustrated in Figure 5. When a walker performs this recrossing behavior, it is eliminated from the simulation due to a recrossing correction.

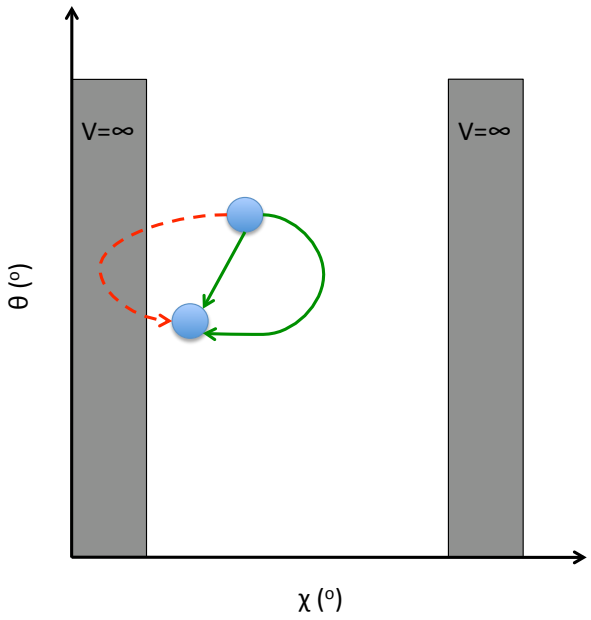

Figure 5: The green lines represent allowed paths for the walker to travel. The red, dashed line represents the path that a walker would take if it were to travel into and the out of the potential energy barrier over one time step.

The probability that a walker performed this recrossing between times τ and $\tau + \delta\tau$ is

$$P_{recross} = \exp\left[-\frac{2m_{eff}\, d(\tau) d(\tau+\delta\tau)}{\delta\tau}\right], \tag{21}$$

where m_{eff} is the effective mass associated with the nodal coordinate and $d(\tau)$ is the walker's displacement from the nodal surface at time τ.[5,10] When the walker crosses a node in θ, the effective mass associated with the coordinate is

$$m_{eff} = \sqrt{\left[\frac{I_{AA}(\tau)+I_{AA}(\tau+\delta\tau)}{2}\right]\left[\frac{I_{BB}(\tau)+I_{BB}(\tau+\delta\tau)}{2}\right]} \tag{22}$$

and in χ, the effective mass is

$$m_{eff} = \sqrt{I_{CC}(\tau) I_{CC}(\tau+\delta\tau)} \tag{23}$$

where $\mathbf{I}(\tau)$ is the instantaneous moment of inertia tensor for a given walker evaluated in the Eckart frame.[16]

H_3^+ RESULTS

TABLE I: The DMC and rigid rotor energies, in cm^{-1}, of selected rotationally excited states of H_3^+ are compared to the results of converged variational calculations.[10]

State	$E_{variational}$ [a]	$E_{DMC} - E_{variational}$ [b]	$E_{RR} - E_{variational}$ [c]
$\left\|1,1,0\right\rangle_+$	64.13	0.84 ± 5.23	-0.36 ± 0.05
$\left\|1,0,0\right\rangle_+$	86.96	1.33 ± 2.01	-0.09 ± 0.10
$\left\|3,3,0\right\rangle_+$	315.35	0.41 ± 4.13	-2.03 ± 0.24
$\left\|3,2,0\right\rangle_+$	428.02	-4.28 ± 1.88	0.80 ± 0.42
$\left\|3,1,0\right\rangle_+$	494.77	-5.60 ± 2.19	3.36 ± 0.56
$\left\|3,0,0\right\rangle_+$	516.88	0.14 ± 2.02	4.34 ± 0.61
$\left\|5,5,0\right\rangle_+$	729.09	-1.80 ± 4.06	-3.55 ± 0.56
$\left\|5,4,0\right\rangle_+$	929.07	-13.13 ± 1.81	4.37 ± 0.79
$\left\|5,3,0\right\rangle_+$	1080.61	-15.69 ± 2.65	14.55 ± 1.09
$\left\|5,2,0\right\rangle_+$	1187.24	-14.69 ± 3.25	23.43 ± 1.33
$\left\|5,1,0\right\rangle_+$	1250.45	-12.83 ± 4.30	29.52 ± 1.49
$\left\|5,0,0\right\rangle_+$	1271.41	1.22 ± 4.69	31.66 ± 1.54
$\left\|10,10,0\right\rangle_+$	2451.77	-6.79 ± 7.55	16.01 ± 2.08
$\left\|10,1,0\right\rangle_+$	4348.79	10.61 ± 10.15	406.05 ± 5.58
$\left\|15,15,0\right\rangle_+$	5092.29	-12.30 ± 7.61	134.45 ± 4.60

[a]The $J \leq 3$ benchmarks are from Dinelli *et al*[17] while the $J \geq 5$ values are from Paniahua *et al*[7].
[b]The reported DMC energies for J=|K| are extrapolations to the $\delta\tau$=0 a.u. limit. The other states are calculated with $\delta\tau$=1 a.u. The error bars are 99% confidence intervals.
[c]The rigid rotor energies were calculated with $\langle B \rangle_0 = 43.44 \pm 0.05$ cm^{-1} and $\langle C \rangle_0 = 20.33 \pm 0.02$ cm^{-1}. The error bars represent 99% confidence intervals.

Table I presents an overview of the results collected for DMC calculations of the rotationally excited states of H_3^+. From the table, it can be seen that the DMC method produces results that are in better agreement with the converged variational calculations than the energy values obtained using a rigid rotor model. The rigid rotor energies that were used to contrast the

effectiveness of our method were calculated via the symmetric top, rigid rotor energy expression, which contains the zero-point vibrationally averaged rotational constants.

(24) $$E_{RR}(J,K) = \langle B \rangle_0 J(J+1) - \left(\langle B \rangle_0 - \langle C \rangle_0 \right) K^2$$

As seen in Table I, the DMC energies are consistently more accurate than the rigid rotor energies when measured against the variational energies. The difference between the DMC energy and the variational energy is less than the difference between the rigid rotor energy and the variational energy. The exception being in cases where the DMC and rigid rotor energies are comparable. The breakdown of this trend can be seen in the high J states of $|10,1,0\rangle_{\pm}$ and $|15,15,0\rangle_{\pm}$, where the differences between the DMC and variational energies are greater than the uncertainties. However, in these states the discrepancy between E_{DMC} and E_{RR} is also most pronounced, so the larger value of E_{DMC} — $E_{variational}$ can be attributed to the larger quanta of rotational excitation in those high J states causing a breakdown in both the rigid rotor and the DMC methods. One of the more interesting pieces of information that can be gathered from looking at this data is that although the fixed-node approximation was employed with the rigid rotor wave functions, DMC was able to capture the rotation-vibration coupling exhibited by the floppy molecules. The rigid rotor approximation neglects such coupling.

To visualize these rotation-vibration couplings in H_3^+, the probability amplitude is projected onto a vibrational coordinate, such as the hyperspherical radius (ρ_{hyper}) or the hyperspherical angle (θ_{hyper}). The hyperspherical radius

(25) $$\rho_{hyper} = \sqrt{S_A^2 + s_{BC}^2}$$

describes the overall size of the molecule. As the molecule experiences rotational excitation, it grows larger due to the effects of centrifugal distortion. The angle θ_{hyper} describes the extent to which the molecular shape deviates from that of an equilateral triangle.

$$\tan(\theta_{hyper}) = \frac{\sqrt{(S_A^2 - s_{BC}^2)^2 + (2\vec{S}_A \cdot \vec{s}_{BC})^2}}{2\left|\vec{S}_A \times \vec{s}_{BC}\right|} \tag{26}$$

In Equations (25) and (26), $\vec{S}_A = d_A \vec{R}_A$ and $\vec{s}_{BC} = d_A^{-1}\vec{r}_{BC}$, where $\vec{R}_A$ is the distance of atom A from the center of mass of B and C, $\vec{r}_{BC}$ is the displacement of atoms B and C, and d_A is the mass weighted pre-factor.[10,18]

$$d_A = \left[\frac{m_A}{\mu}\left(1 - \frac{m_A}{M}\right)\right]^{1/2} \tag{27}$$

In Equation (27), μ is the reduced mass of the three body system, and M is the total mass.[18] Figure 6 shows the projection of the probability distributions for various rotationally excited states onto these coordinates. The hyperspherical radius distribution is more affected by rotational excitation than the hyperspherical angle. As the amount of energy in the system, J, increases, the distributions shift to larger values of ρ_{hyper}.

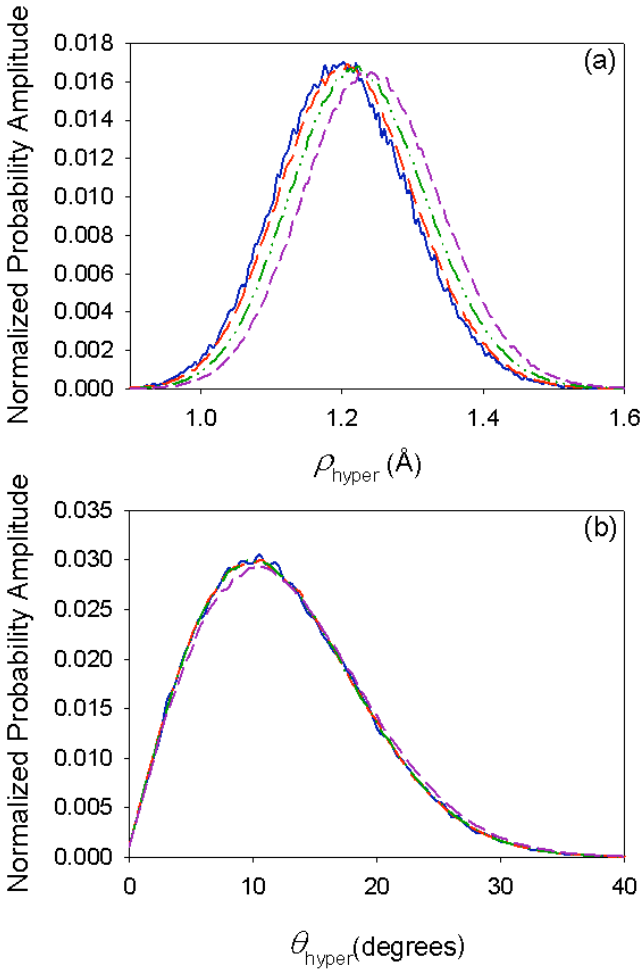

Figure 6: Plots of the projections of the DMC probability amplitude onto (a) ρ_{hyper} and (b) θ_{hyper} for the $|0,0,0\rangle$ (blue), $|5,5,0\rangle_+$ (red), $|10,10,0\rangle_+$ (green), and $|10,1,0\rangle_+$ (purple) states of H_3^+.[10] Reprinted with permission from [A. S. Petit, B. A. Wellen, and A. B. McCoy, J. Chem. Phys. **136**, 074101 (2012)]. Copyright [2012].

INTERNAL CHECKS

In order to better understand the cause of the deviations between the DMC and benchmark energies of the systems, the dependence of the results on the size of the time step, $\delta\tau$, was investigated by comparing the energies calculated at various time steps from $\delta\tau$=0.5 to 5 a.u. As shown in Figure 7, larger time step dependence is observed in those states with greater

rotational excitation; the representative states have the property J=|K|. It can be seen that extrapolating to the δτ=0 limit provides energies that are close to the benchmark values.

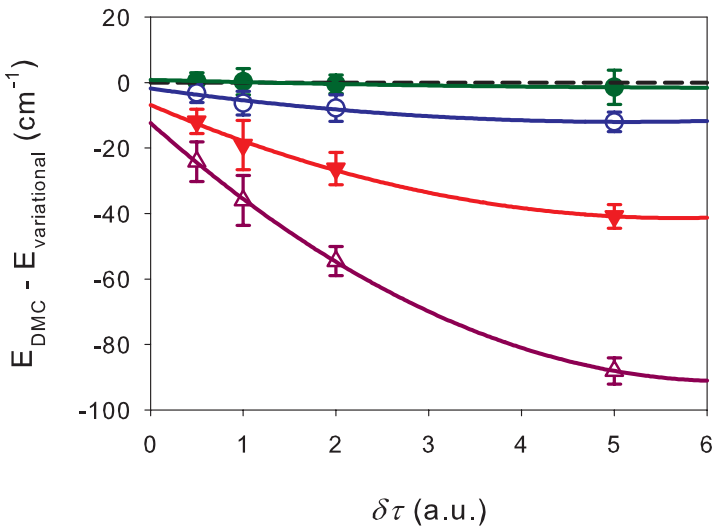

Figure 7: The time step dependence of $E_{DMC} - E_{variational}$ calculated for the $|1,1,0\rangle_+$ (green), $|5,5,0\rangle_+$ (blue), $|10,10,0\rangle_+$ (red), and $|15,15,0\rangle_+$ (purple) stated of H_3^+.[10]
Reprinted with permission from [A. S. Petit, B. A. Wellen, and A. B. McCoy, J. Chem. Phys. **136**, 074101 (2012)]. Copyright [2012].

As rotational excitation increases, the overall size of the nodal regions decreases, as illustrated in Figure 8.

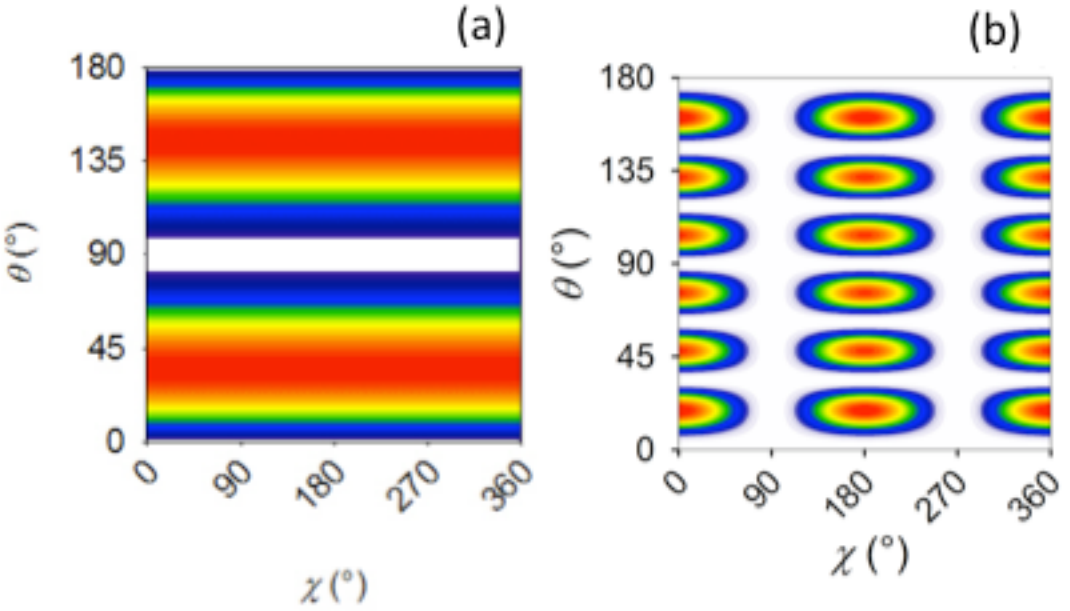

Figure 8: The wave function of the J=1 state is shown in (a), while (b) is the wave function of a J=6 state.[10]

This can explain why the time step dependence became more pronounced in the higher J states in Figure 7, because smaller nodal regions lead to increased contact between the infinite potential barrier and the walker.

When the dependence of energetic accuracy on nodal region is investigated, an interesting trend is observed. Any dependence of energy on the choice of nodal region in which the DMC simulation is performed is evidence of a deficiency in the method. Recall that because $\hat{H}\Psi=E\Psi$ much be satisfied everywhere in configuration space, the energies in all the regions should be equal if the nodes are properly defined and the infinite potentials around those nodes are properly enforced. When DMC calculations are performed in the outer nodal regions (those regions where $\theta=0$ or 180^{o}), the difference increased between the calculated DMC energy and the benchmark variational energies. Figure 9(a) shows the energy difference for the $|10,1,0\rangle_{+}$ state with a time step of $\delta\tau = 1$ a.u. and 9(b) shows the energy difference of that state at the $\delta\tau = 0$ a.u. limit. The extrapolation to the time step limit decreased the difference between the energy

values, but still demonstrates a difference between the outer and central (where θ either equals or contains 90°) nodal regions.

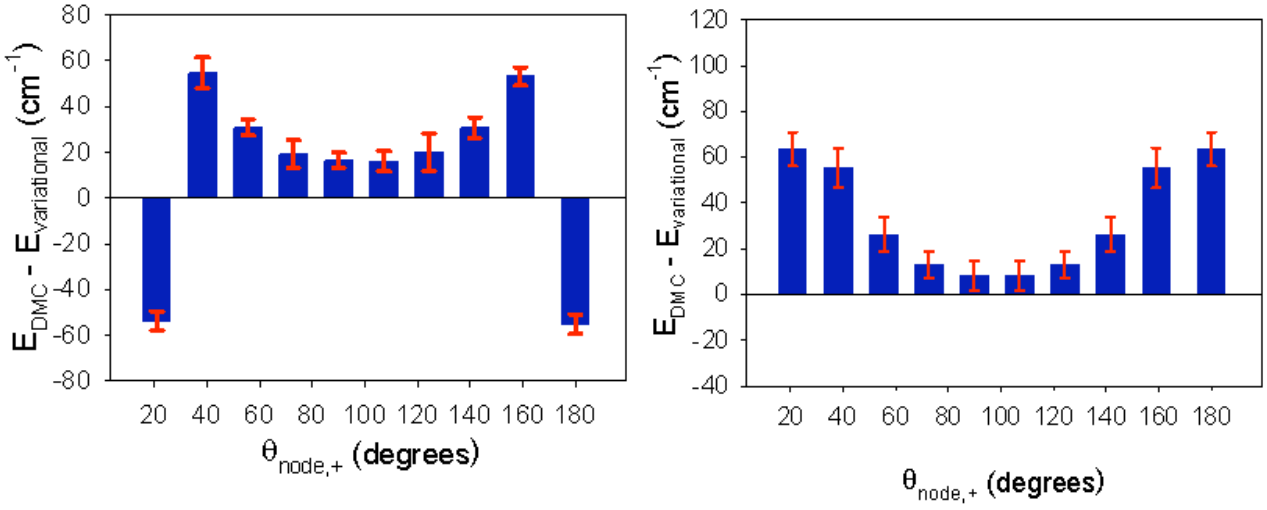

Figure 9: $E_{DMC} - E_{variational}$ for H_3^+ calculated in representative nodal regions for the $|10,1,0\rangle_+$ state. Figure 9(a) shows the results of the calculation with $\delta\tau$=1 a.u. while 9(b) shows the results after an extrapolation to the $\delta\tau$=0 a.u. limit.[10]
Reprinted with permission from [A. S. Petit, B. A. Wellen, and A. B. McCoy, J. Chem. Phys. **136**, 074101 (2012)]. Copyright [2012].

The rotational nodal surfaces lie on a sphere. The outer nodal regions can be thought of as being located at one of the poles of the sphere where a small displacement in angle generates a larger displacement than χ would produce at the central nodal region. This is illustrated in Figure 10, where the North and South Poles represent the outer nodal regions.

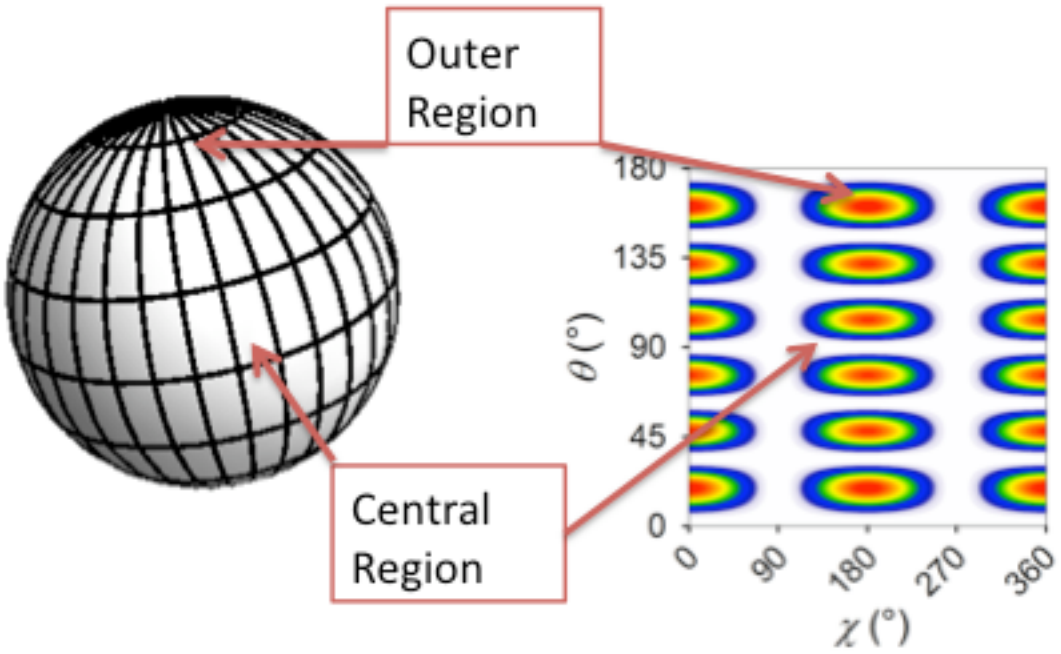

Figure 10: The nodal surface can be thought of as a globe, where the latitude lines are in θ and the longitude lines are in χ. A small shift in χ at the North Pole would produce a larger displacement than the same angle would produce at the Equator.

The effective size of an outer nodal region is also much smaller than a region at the center of the surface. Both of the aforementioned factors cause the walkers to encounter the perimeter of the nodal surface more frequently than the walkers in a central nodal region. The decreased size of the surface increases the probability of recrossing, much like how increased rotational excitation leads to increases in recrossing. Therefore, any deficiency in the recrossing correction becomes more pronounced at the outer nodal regions.[10]

Now recognizing how recrossing is affected by the choice of nodal region, we can gain even more insight into the data presented in Figure 9. The recrossing correction is dependent on the size of the time step. In Figure 9(b), $\delta\tau=0$, so the variations of energy amongst the different nodal regions cannot be attributed to a deficiency in the recrossing correction. This shows that other factors are contributing to the breakdown of the method. This deficiency may be attributed to the vibrational behavior of the system that cannot be accounted for in our approach.[10]

H_2D^+ RESULTS

H_2D^+ is a highly asymmetric top molecule. Its asymmetry parameter, κ, is close to 0 whereas the limits of purely symmetric top molecules fall where κ is equal to ±1. With the vibrationally averaged rotationally constants used in this study, κ of H_2D^+ is equal to -0.07.

(27) $$\kappa = \frac{2\langle B\rangle_0 - \langle A\rangle_0 - \langle C\rangle_0}{\langle A\rangle_0 - \langle C\rangle_0}$$

TABLE II. The DMC and rigid-rotor energies, given in cm^{-1}, as compared to the results of converged variational calculations for representative rotationally excited states of H_2D^+.[3]

State	$E_{variational}$[a]	E_{DMC}- $E_{variational}$[b]	E_{RR}-$E_{variational}$[c]
$3_{0,3}$	251.37	0.49 ± 5.12	0.52
$3_{1,2}$	326.15	-1.77 ± 5.79	1.81
$3_{2,1}$	376.35	-0.19 ± 5.00	2.70
$3_{3,0}$	459.84	-1.35 ± 6.17	4.16
$6_{1,5}$	991.01	-0.67 ± 6.73	11.72
$6_{3,3}$	1206.12	-1.02 ± 5.58	27.87
$6_{4,2}$	1302.33	-3.91 ± 5.30	31.83
$6_{5,1}$	1455.04	-0.34 ± 7.10	40.18
$10_{1,9}$	2301.80	1.83 ± 4.62	51.75
$10_{3,7}$	2790.09	-20.88 ± 7.11	121.93
$10_{5,5}$	3048.45	-16.08 ± 6.56	181.71
$10_{7,3}$	3387.85	-11.54 ± 5.47	216.02
$10_{9,1}$	3905.28	-0.47 ± 9.12	307.52
$10_{10,0}$	4198.58	0.99 ± 6.56	384.28

[a]The benchmark values are from Sochi and Tennyson.[9]

[b]The DMC calculations were performed in an inner nodal region adjacent to or containing θ=90° and the energies are extrapolations to the δτ=0 limit. The error bars are 99% confidence intervals.

[c]The E_{RR} are calculated with the vibrationally averaged rotational constants $\langle A\rangle_0$=43.400 cm^{-1}, $\langle B\rangle_0$=29.115 cm^{-1}, and $\langle C\rangle_0$=16.603 cm^{-1}. The error bars are 99% confidence intervals.

Table II provides an overview of the results obtained from the fixed-node DMC calculations of select rotationally excited states of H_2D^+. It is important to note that all of the calculations were performed in an inner nodal region adjacent to or containing θ=90°. This value of θ was chosen due to the better energetic accuracy of the inner nodal regions seen in the

previous study of H_3^+. Overall, excellent agreement can be seen between the DMC and the variational energies. Particularly, the J=3 and J=6 states produce a DMC energy that is in exact agreement with the benchmark values within statistical uncertainties. The J=10 states with larger values K_A or K_C are also in excellent agreement with the variational energies. Those states with intermediate values of K_A and K_C display statistically significant deviations from the benchmark values, but this deviation never exceeds 1% of the rotational energy.

Also seen in Table II are the asymmetric top rigid rotor energies. These energies are obtained by finding the eigenvalues of the rigid rotor Hamiltonian in Equation (1) using a symmetric top basis set. The corresponding wave functions are used to obtain the nodal surfaces for the fixed-node DMC study in roughly the same manner as they were obtained in the H_3^+ study. The nodal surfaces in H_2D^+, however, cannot be described with straight lines in θ and χ, as was the case for H_3^+. A more tedious, but relatively simple, method is used to define the nodal region. The four corners of the nodal region are first found in θ and χ. Then, the zeroes are found in either θ or χ along each of the four connecting boundaries of the surface for a specified number of points using the "FindRoot" command in Mathematica. This provides the nodal region for the DMC study.

For J=3, the rigid rotor energies, like the DMC energies, are comparable to the variational energies. However, as the value of J is increased to 6 and to 10, the deviation of the rigid rotor energies from the variational energies is considerably larger than the value of $|E_{DMC} - E_{variational}|$. For all but one of the J=10 states considered in the study, $|E_{RR} - E_{variational}|$ exceeds over 100 cm^{-1}. While the rigid rotor approximation produces energy values that are far from accurate, the wave functions obtained via this approximation, when applied to the DMC simulations, produce incredibly accurate results. If we compare the contour plots of the wave functions produced by

the rigid rotor approximation and by the DMC simulation, it can be seen that DMC is able to pick up on the shape, and even the bimodal character of the wave function. Recall, that the only input the simulation receives is the definition of the boundaries of the nodal region as functions of θ and χ.

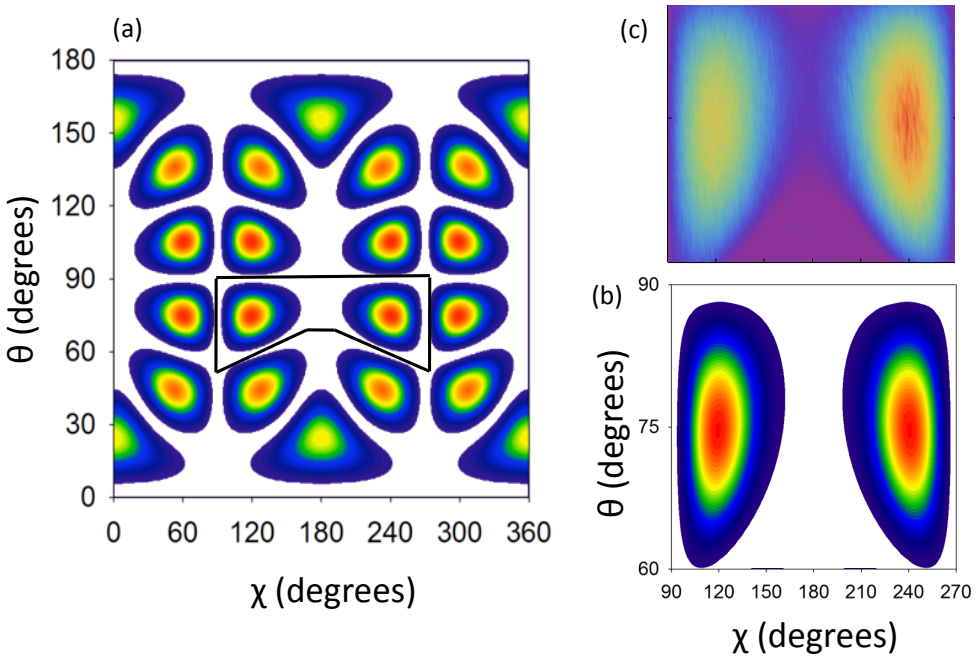

Figure 11: The rigid rotor wave function of the $6_{5,1}$ state of H_2D^+ is shown in (a). The outlined region in (a) is represented in (b). The region in (c) is the outlined nodal region produced by DMC.[3]

Despite increased complexities in the nodal structure and the recrossing correction, the DMC energies obtained for the asymmetric tops are comparable to if not more accurate than those results obtained in the symmetric top study. This demonstrates the strength of our DMC methodology in that it is able to accommodate the additional complicated factors that are present in asymmetric top systems.

INTERNAL CHECKS

Because H_2D^+ is an asymmetric top, and its nodal structure exhibits significant curvature, the recrossing correction implemented in the H_3^+ study was modified to better describe the locations of the walker and the nodal surface. The new equation of $P_{recross}$ still closely follows the physical meaning of Anderson's original expression and corrects for the curvature present in the nodal surfaces.[3-5]

The data in Table II also provides an indication of the time step dependence of the DMC energies. The magnitude of this dependence increases as rotational excitation increases. While the DMC energies reported here were extrapolated to the $\delta\tau=0$ limit, as described in the previous part, the energies in this limit generally were not statistically significantly different than those at $\delta\tau=0.5$.

As discussed earlier, despite the breakdown of the rigid rotor approximation when it comes to determining the energy of the system, the nodes in the asymmetric top rigid rotor wave function are able to provide a suitable set of nodal surfaces to be used in the fixed-node DMC calculations. Even by using a strictly rotational picture to define the nodal surface, it can be seen that the DMC simulation is able to capture rotation-vibration coupling in the highly fluxional system.

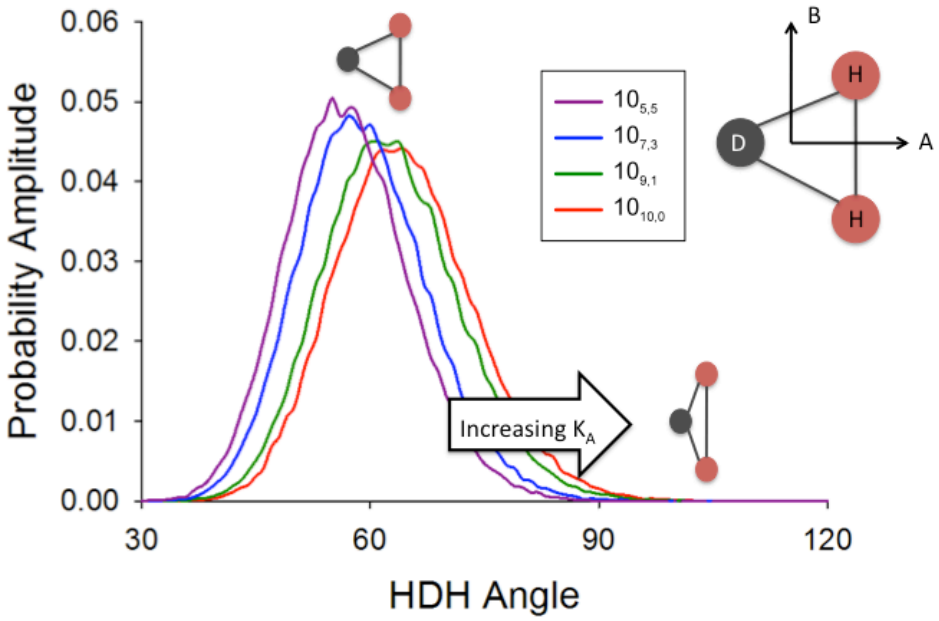

Figure 12: The projection of the DMC probability amplitude onto the θ_{HDH} vibrational coordinate for representative J=10 states of H_2D^+.
Reprinted with permission from [A. S. Petit, B. A. Wellen, and A. B. McCoy, J. Chem. Phys. **138**, 034105 (2013)]. Copyright [2013].

Figure 12 examines four rotationally excited states, each with J=10. As the value of K_A increases, the probability distributions shift to larger values of the HDH angle. K_A describes the projection of the angular momentum onto the body-fixed A-axis. This is the axis that bisects the HDH angle. The vibrational components of the DMC wave functions are therefore able to respond to rotational excitation. It is because of this response of the DMC wave function in the vibrational degrees of freedom to the nodes placed in the rotational coordinates that the DMC energies are in much better agreement with the variational energies than the rigid rotor energies.[3]

CONCLUSION

Fixed-node Diffusion Monte Carlo is an effective approach for obtaining the energies and wave functions of the rotationally excited states of fluxional symmetric and asymmetric top molecules. It has been shown that the use of the rigid rotor nodal surfaces allowed for calculations of the energies of rotationally excited states of better accuracy than the rigid rotor approximation alone. It has also been demonstrated via the projections of the DMC probability amplitude onto the vibrational coordinates that the method is capable of providing insight into the rotation-vibration coupling present in these types of systems.

The fixed-node DMC methodology developed and employed in these studies provides a general approach for describing the rotationally excited states of fluxional molecules. However, there are some limitations to this method. First, a global potential energy surface must exist in order for the simulation to be performed. And, a separate calculation must be performed for each excited state individually.

The work performed thus far in these DMC studies can be utilized in further investigations of other fluxional molecules. For example, the rotationally excited states of H_5^+ are of interest, as well as the reaction path between H_3^+ and H_2 to form H_5^+. Fixed-node Diffusion Monte Carlo can provide further insights into these molecules and their reaction dynamics.[3,10]

REFERENCES

[1]T.P. Snow and B.J. McCall, Annu. Rev. Astron. Astrophys. **44**, 387 (2006).
[2]McCall, B.J., Geballe, T.R., Hinkle, K.H., Oka, T. *The Astrophysical Journal*. **522**, 338-348 (1999).
[3]A. S. Petit, B. A. Wellen, and A. B. McCoy, J. Chem. Phys. **138**, 034105 (2013).
[4]J. B. Anderson, J. Chem. Phys. **63**, 1499 (1975).
[5]J. B. Anderson, J. Chem. Phys. **65**, 4121 (1976).
[6]O.L. Polyansky and J. Tennyson, J. Chem. Phys. **110**, 5056 (1990).
[7]A. Aguado, O. Roncero, C. Tablero, C. Sanz, and M. Paniagua, J. Chem. Phys. **112**, 1240 (2000).
[8]W. Cencek, J. Rychlewski, R. Jaquet, and W. Kutzelnigg, J. Chem. Phys. **108,** 2831 (1998).
[9]T. Sochi and J. Tennyson, Mon. Not. R. Astron. Soc. **405**, 2345 (2010).
[10]A. S. Petit, B. A. Wellen, and A. B. McCoy, J. Chem. Phys. **136**, 074101 (2012).
[11]A. B. McCoy, Int. Rev. Phys. Chem. **25**, 77 (2006).
[12]A. S. Petit and A. B. McCoy, J. Phys. Chem. A **113**, 12706 (2009).
[13]A.B.McCoy, Chem. Phys. Let. **321**, 71-77 (2000).
[14]M.A. Suhm and R.O. Watts, Phys. Rep. **204**, 293 (1991).
[15]Bernath, P.F., *Spectra of Atoms and Molecules*, Oxford University Press: New York, 2005.
[16]A.B. McCoy, C.E. Hinkle, A.S. Petit. Studying Properties of Floppy Molecules Using Diffusion Monte Carlo. In *Advances in Quantum Monte Carlo*; Tanaka, S., Rothstein, S.M., and Lester, W.A., Ed.; Oxford University Press: Washington D.C., 2012; p.145.
[17]B.M. Dinelli, L. Neale, O.L. Polyansky, and J. Tennyson, J. Mol. Spectrosc. **181**, 142 (1997).
[18]R.T. Pack and G.A. Parker, J. Chem. Phys. **87**, 3888 (1987).